15 Aug 2023

Defect Generation Mechanisms In Silica Under Intense Electronic Excitation By Ion Beams Below 100 K: Interplay Between Radiative Emissions

M. L. Crespillo

Joseph T. Graham
Missouri University of Science and Technology, grahamjose@mst.edu

W. J. Weber

F. Agulló-López

Recommended Citation

M. L. Crespillo et al., "Defect Generation Mechanisms In Silica Under Intense Electronic Excitation By Ion Beams Below 100 K: Interplay Between Radiative Emissions," *Acta Materialia*, vol. 255, article no. 119097, Elsevier; Acta Materialia, Aug 2023.
The definitive version is available at https://doi.org/10.1016/j.actamat.2023.119097

Acta Materialia 255 (2023) 119097

Contents lists available at ScienceDirect

Acta Materialia

journal homepage: www.elsevier.com/locate/actamat

Defect generation mechanisms in silica under intense electronic excitation by ion beams below 100 K: Interplay between radiative emissions

M.L. Crespillo [a,b,*], J.T. Graham [c,*], W.J. Weber [a], F. Agulló-López [b,*]

[a] Department of Materials Science and Engineering, University of Tennessee, Knoxville, Tennessee 37996, United States
[b] Centro de Microanálisis de Materiales, CMAM-UAM, Cantoblanco, Madrid 28049, Spain
[c] Department of Nuclear Engineering and Radiation Science, Missouri University of Science and Technology, Rolla, Missouri 65409, United States

ARTICLE INFO

Keywords:
Fused silica
Ion irradiation
In situ
Luminescence
Lattice defects

ABSTRACT

Ion-beam effects on bulk silica at low temperature have been studied with the aim of understanding the routes and mechanisms leading from the initial generation of free carriers and self-trapped excitons (STEs) to the production of two stable defect structures in irradiated silica, non-bridging oxygen hole centers (NBOHCs) and oxygen deficient centers (ODCs). Ion beam induced luminescence (ionoluminescence, *IL*) spectra were obtained using 3 MeV H, 3.5 MeV He, 19 MeV Si, and 19 MeV Cl ions and a range of cryogenic irradiation temperatures from 30 to 100 K. The kinetic behavior of three emission bands centered at 1.9 eV (assigned to NBOHCs), 2.1 eV (assigned to the intrinsic decay of STEs), and 2.7 eV (assigned to ODCs) reveal the physical origin of these emissions under intense electronic excitation. The creation of NBOHCs is governed by a purely electronic mechanism. The kinetics curve of the NBOHC band shows two main contributions: an instantaneous (beam-on) contribution, followed by a slower fluence- and temperature-dependent process correlated with the concentration of STEs. The beam-on contribution is proportional to deposited ionization energy. The growth of the ODC band is linear in fluence up to around 2×10^{12} cm^{-2}. The growth rate is independent of temperature but proportional to the number of radiation-induced oxygen vacancies per ion, showing, unambiguously, that the 2.7 eV emission can be associated with ODCs created in an excited state.

1. Introduction

Amorphous a-SiO_2 (silica) is an insulator ubiquitous in many fields of science and technology such as physics, chemistry, geology, earth sciences, microelectronics, and optics. The material comprises SiO_4 tetrahedra connected through the O vertices (bridging oxygen). Though the stability of the SiO_4 tetrahedron gives rise to short-range order, random variation in the Si-O-Si bond and bond lengths lead to loss of long-range order and a glassy structure. The electronic energy gap is around 9 eV and arises from transitions between O ($2p^2$) orbitals in the valence band (VB) and Si and O s, p, and d orbitals in the conduction band (CB). Aside from classical applications based on its wide window of optical transparency, high electrical resistivity, and thermally insulating properties, novel applications are being developed in micro-photonics and microelectronics [1–3], and nuclear technologies [4–6]. Many of these applications either rely on or are hindered by the properties of point defects. Point defects can be introduced during growth or through external influences such as ionizing irradiation. Moreover, silica is a model system for studying the complex variety of atomic and electronic defects in amorphous insulators. Consequently, considerable research activity has been devoted to understanding the atomic and electronic structure of its defect centers, as emphasized in reviews [7–9] and books [10,11]. A class of techniques used to study defects in silica is optical spectroscopy. Optical spectroscopy techniques typically offer high sensitivity to defects and have been widely used in the study of defect centers in insulating materials [10]. Characterization studies performed on silica over the years have used a large variety of irradiation sources, such as UV light [11,12], synchrotron radiation [12,13], electron irradiation [14,15], gamma radiation [16,17], neutrons [18–20] and ion beams [21–25]. Experiments using swift heavy ions (mass>4 amu and ~MeV/amu energy scales) to study the optical properties of silica, e.g. luminescence and absorption, are comparatively scarce [26–29]. Previous studies on the effects of heavy ion irradiation on luminescence spectra and spectral kinetics [30,31] have shown promise for offering new insights into carrier transport and recombination mechanisms.

In this work, we present the IL spectral response from high-energy

* Corresponding authors.
E-mail addresses: miguel.crespillo@uam.es (M.L. Crespillo), grahamjose@mst.edu (J.T. Graham), fal@uam.es (F. Agulló-López).

https://doi.org/10.1016/j.actamat.2023.119097
Received 12 March 2023; Received in revised form 18 May 2023; Accepted 15 June 2023
Available online 16 June 2023

(E > 0.1 MeV/amu) light and heavy ions at cryogenic temperatures (<100 K). These ions dissipate the majority of their energy through electronic excitation (as described by the electronic stopping power, S_e). At the energies and stopping powers studied, high electronic carrier densities are achieved that are comparable to, and in some cases greater than, those produced by high power pulsed lasers ($\sim 10^{19}$–10^{22} e-h/cm^3) [32]. This fact is both relevant to nuclear fusion applications and also complements research on luminescence from lower energy density ionizing and non-ionizing radiation sources. *IL* combines the high sensitivity of luminescence techniques with the broad excitation spectrum and intense electronic density achievable with ion irradiation, allowing one to study essentially all optically active transitions [33]. Another advantage of *IL* is the possibility of controlling the ratio of the collisional versus ionization processes by modifying the mass and energy of the projectile ions [25,31]. *IL* experiments are not a simple variant of more conventional luminescence techniques such as photoluminescence (PL) or cathodoluminescence (CL). They constitute an *in-situ* and *real--time* technique that, depending on ion mass and energy, offers a wide range of surface penetration depths and excitation densities. They enable one to monitor the evolution of spectral components with time and ion fluence. Penetration depth can be varied from less than one micron to tens of microns through an appropriate choice of ion energy. Thus, in contrast to cathodoluminescence (CL) or UV light photoluminescence (PL), surface effects can be minimized [34,35].

It is now well established that the luminescence emissions of amorphous silica under various irradiation sources contain three main bands, a blue band at 2.7 eV, likely attributable to oxygen deficient centers (ODCs) [7,8,18,26,36,37], a green band at 2.1 eV due to self-trapped excitons (STEs) [11,38-41], and a red band at 1.9 eV due to non-bridged oxygen hole centers (NBOHCs) [7,8,21,22,31,42,43]. The 1.9 eV emission has been attributed to the presence of OH groups, incorporated in silanol (Si-OH) molecules. Depending on the manufacturing process, these OH impurities may be prevalent and determine many of the optical properties of the glass. NBOHCs are generated through scission of the silanol bond [31]. Another efficient mechanism for generating NBOHCs involves the scission of strained (≡Si−*O*−Si≡) bonds [30,42,43], as was shown in pioneering papers by R.A.B Devine [44,45] and a number of other authors. It should be noted that this mechanism requires no impurities to occur. The structure of the NBOHCs and several other centers are given in **Suppl. Fig. 1**.

The emission band centered at 2.7 eV is associated with a particular type of oxygen vacancy, the ODC(II) center. ODC(I) refers to a relaxed, neutral oxygen vacancy, whereas ODC(II) refers to the non-relaxed diamagnetic oxygen vacancy. The 2.7 eV band corresponds to the ODC(II) triplet-to-singlet transition ($T_1 \rightarrow S_0$). A 4.4 eV band is associated to the ODC(II) singlet-to-singlet transition ($S_1 \rightarrow S_0$) [7,37,46-50].

It is pertinent to point out that the STE emission at 2.1 eV overlaps in energy considerably with the 1.9 eV and 2.7 eV bands, particularly around or above RT. Clear unfolding of those bands is difficult to achieve at elevated temperatures. The use of cryogenic irradiation temperatures has allowed for robust line shape fitting and subsequent quantification of emission intensities [32]. Recently, a correlation was observed between the green and red spectral regions under synchrotron irradiation using a variety of silica samples grown by different procedures and presenting different structural features [13]. The correlation has been attributed to a competition between STEs and NBOHCs, but the model in that study has not yet been corroborated. Detailed quantitative analysis of the competition reported in [13] might be hindered by difficulty of separating the highly overlapped blue and green spectral components, which were jointly considered in that work.

IL has recently been used in our laboratory to successfully investigate the emission spectra and the generation kinetics of different electronic and lattice defects generated by intense electronic excitation under ion-beam irradiation in several crystalline complex oxides, as well as, silica and quartz [25,30-33,51-58].

In relation to the objective of this work, it is worth remarking that previous experiments supporting the assignment of the green emission at 2.1 eV to STEs have been mostly performed at low temperatures using intense electronic excitation (i.e. laser or electron pulses) where no structural damage is expected. However, experiments dealing with ion beam irradiation, where structural damage is produced, have not been reported so far. An exception is a recent work dealing with the *IL* at very low fluence [32] where the initial radiative yield of the STE emission, as a function of ion mass and energy of the projectile ion, was investigated in detail. It has been demonstrated that the initial yield of that band is the result of a competition of several processes including: STE formation, Auger recombination, thermal dissociation, and hopping migration. The aim of the present work has been to monitor the evolution and interplay between the STE, NBOHC and ODC emission centers during low-temperature, high-energy, heavy ion-beam irradiation. The routes and mechanisms that take the SiO_2 network from its initial state, populated mostly by STEs, to its final, defective state is our primary focus.

2. Experimental methods

2.1. Low-OH content samples and ion irradiation conditions

Two-side polished, IR-grade, fused silica (SiO_2) samples from Crystran Ltd. (Poole, UK) [59] were used in this study. The samples had an [OH] concentration less than 10 ppm. Those were the same as the "dry silica" glasses used by Bachiller-Perea et al. [30]. Metal impurities were in the lower ppm range. The samples were irradiated in the Ion Beam Materials Laboratory (IBML) at the University of Tennessee, Knoxville [60]. Optically polished plates 18 mm in diameter and 1 mm in thickness were cut with a diamond pen and cleaned with trichloroethylene and acetone. A variety of projectile ions and energies were selected for irradiation, namely 3 MeV H^+, 3.5 MeV He^+, 19 MeV Si^{6+} and 19 Cl^{6+} MeV to cover a broad range of electronic (S_e) and nuclear (S_n) stopping powers. Beam slits were used to define a square irradiation area between 1×1 mm^2 and 2.5×2.5 mm^2 (depending on ion and energy). The beam was rastered over the slits to maintain beam homogeneity within 10%. Particle fluxes were between 4×10^{11} and 4×10^{12} particles cm^{-2} s^{-1}. Low fluxes were used to minimize undesirable ion beam heating [61]. The relevant irradiation parameters, including overall electronic excitation rates, *G*, are summarized in Table 1. Note that the electron-hole densities used in this work are comparable to those achieved in most picosecond (ps)-pulsed laser experiments.

2.2. SRIM simulations

Electronic stopping powers, projected ion ranges (R_p), ionization energy (E_{ioniz}), energy transferred to target atoms ($E_{recoils}$), and number of generated oxygen vacancies, included in Table 1, were calculated using the Stopping and Range of Ions in Matter (SRIM) binary collision approximation (BCA) software using full-cascade simulations (version 2012) [62,63]. **Suppl. Fig. 2** shows the electronic and nuclear stopping power profiles versus depth inside fused SiO_2 for the irradiations discussed in this work. Threshold displacement energies were 15 eV and 28 eV for the Si and O atoms, respectively. A density of 2.2 g cm^{-3} for SiO_2 was assumed. The single-ion excitation rate, $N_{e\text{-}h}$, or average number of e-h pairs generated by a single ion can be approximated by the expression [64,65]

$$N_{e-h} = \frac{E_{ioniz}}{I} \cong \frac{E_{ioniz}}{2.5E_g} \quad (1)$$

where: E_{ioniz} is the energy deposited into the electronic system per incident ion (equivalent to integrating the electronic stopping power along the ion path), *I* is the effective ionization energy, and E_g is the band-gap energy of SiO_2 ($E_g = 9.0$ eV). The overall electronic excitation rate, *G*, is given by

Table 1
Irradiation parameters calculated using SRIM (version 2012) full-cascade simulations. F_{avg} is the average incident particle flux. $E_{recoils}$ represents the total energy transferred per incident ion to target atoms (Si and O), and *Total oxygen vacancies* is the total number of oxygen vacancies produced per incident ion integrated along R_p. (A detailed description on the parameters can be found in **Experimental methods** section).

Ion, Energy (MeV)	R_p (μm)	$S_{e,\ max}$ (keV/nm)	E_{ioniz} (MeV)	F_{avg} ($\times 10^{12}$ cm^{-2} s^{-1})	$N_{e\text{-}h}$ ($\times 10^5$ e-h/ion)	G ($\times 10^{17}$ e-h $cm^{-2}s^{-1}$)	$\rho_{e\text{-}h}$ (e-h cm^{-3})	$E_{recoils}$ (MeV)	Total oxygen vacancies
H, 3	93.5	0.08	2.99	3.00	1.33	4.00	4.53×10^{18}	1.89×10^{-3}	19.20
He, 3.5	14.6	0.34	3.49	3.80	1.55	5.90	3.38×10^{19}	0.01	103.18
Si, 19	8.00	3.48	18.63	0.46	8.28	3.81	3.30×10^{20}	0.37	2707.68
Cl, 19	7.50	4.15	18.47	0.45	8.21	3.70	3.49×10^{20}	0.53	3678.90

$$G = N_{e-h}F = \frac{E_{ioniz}\ F}{2.5E_g} \quad (2)$$

F is the particle flux.

The density of excited *e–h* pairs (ρ_{e-h}) was estimated by dividing N_{e-h} by the excitation volume, approximated as a cylinder of length R_p, equal to the ion range, and an excitation radius of ~10 nm, corresponding to the maximum range of delta electrons. In reality, the excitation density varies as a function of distance from the track core. However, considering that the bulk of the electronic collisional cascade occurs within the first 10 nm, ρ_{e-h} is a useful mean parameter for making a relative comparison of electronic excitation density for each of the ions.

2.3. Temperature control

The specimens were mounted on a closed-cycle helium cryostat (Advanced Research Systems, Inc. model DE-204-SF) in a beamline endstation under vacuum maintained at or below 6.7×10^{-7} Pa pressure. Specimen temperatures were monitored by means of a silicon diode sensor mounted onto the sample holder. Commercial vacuum compatible thermal grease with high efficiency at cryogenic temperatures was used to improve thermal contact and temperature uniformity between the bottom of the sample and the sample holder. To reduce charge accumulation on the sample surface during the irradiation, double-sided Cu tape was applied over the edges of the sample surface and sample holder. Nominal irradiation temperatures were 33, 45, 55, 65, 75, 85, 90, and 106 K.

2.4. Ion beam luminescence (IL) acquisition and data analysis

Light was collected at 150° with respect to the beam direction through a sapphire window using a focusing lens and fiberoptic cable. The light was analyzed in a spectrograph (Acton SP-2556) with 0.2 nm spectral resolution and liquid nitrogen cooled charged coupled device (CCD) configured for UV–vis spectral analysis. Spectra were acquired in 200–1200 ms intervals, depending on the beam current and temperature. Further details of the optical set-up are provided in [25,32,33,52,60]. A schematic diagram of the *in-situ* experimental setup is shown in **Suppl. Fig. 3.** The IL intensity was normalized using several experimental parameters (spectrometer entrance slits apertures, acquisition time, luminescent area and incident particles flux) with the aim of quantitatively comparing the luminescent yields from different ion beams.

Data analysis of the *IL* spectra is described elsewhere [32]. Raw spectra comprised ordered pairs of wavelengths and photon counts binned by wavelength (λ, C_λ). After converting from wavelength to energy binning using an area preserving transformation, a model comprised of split Voigt profiles was fit to the spectra using the Fityk software [66]. After an initial fitting step to establish the line shape parameters, the shape parameters were fixed and only the peak heights were allowed to vary. Thus, all *IL* spectra for the entire set of temperatures under study could be decomposed into three asymmetric components with only three degrees of freedom (peak heights). Fourier analysis of the residuals revealed that the maximum low frequency component (attributable to error in the model) was generally less than twice the RMS noise. Uncertainties on the fitting parameters were determined using the method described in [67], and the uncertainties of derived values were propagated using the quadrature method.

3. Results and discussion

3.1. Ionoluminescence spectra and kinetics for ion-beam irradiation at cryogenic temperatures

The first experimental parameters to be discussed are the projectile ion mass and irradiation temperature. Although several ions have been used in this research, two representative cases: 3.5 MeV He, a light ion, and 19 MeV Si, a heavy ion, offer a suitable starting point for discussion.

A) Light ion irradiations:

IL spectra acquired for 3.5 MeV He at the lowest irradiation temperature (36 K) are shown in Fig. 1**(a)**. For low irradiation fluences (below 1×10^{12} $cm^{-2}s^{-1}$), essentially one broad band peaked at 2.1 eV, corresponding to the STE center, is observed. At higher fluences and at higher temperatures, two additional contributions at 1.9 eV (NBOH centers) and at 2.7 eV (ODC(II) centers) appear. The ODC(II) singlet-to-singlet transition ($S_1 \rightarrow S_0$) emitting at around 4.4 eV [7,37,46-48] is out of the measurable spectral range of these experiments. Spectra corresponding to 3.5 MeV He at 85 K for several fluences are shown in Fig. 1 **(b)**. The IL spectra look similar to those measured at 36 K for all fluences, both in shape and intensity. Fig. 1**(c)** presents the IL spectra for 3 MeV H at several fluences and at the lowest temperature (33 K). As with 3.5 MeV He, a broad band is observed around 2.1 eV, corresponding to the STE emission center. However, in contrast to 3.5 MeV He, much higher fluences (on the order of 10^{14} $cm^{-2}s^{-1}$) are needed to see the appearance of the other two emission bands.

The kinetic evolution of the radiative yields (area under the IL curve) associated with each emission band are shown in Fig. 2 for the case of 3.5 MeV He at 36 K. A magnified plot of the low fluence regime is shown in Fig. 2**(a)**, while the behavior at higher fluences is illustrated in Fig. 2 **(b)**. The main features are as follows. The dominant band centered at 2.1 eV (STE centers) rapidly decays with fluence as previously shown and discussed in [32]. At the same time, the band centered at 1.9 eV (NBOH centers) exhibits an initial, near instantaneous (beam-on), non-zero yield. With increasing fluence, the yield increases gradually but remains within an order of magnitude of its initial value, even after higher fluences are reached ($<10^{14}$ cm^{-2}). In contrast, the band centered at 2.7 eV (ODC(II)) has an initial yield of zero (to within uncertainty), and grows with fluence. The growth is approximately linear up to around 3–4 $\times$ 10^{13} cm^{-2} (Fig. 2**(a)**) after which it becomes the most intense component in the spectra. Above 10^{14} cm^{-2} the ODC(II) emission yield levels off, reaching a saturation regime around 6×10^{14} cm^{-2} **(**Fig. 2**(b))**. The kinetics curves for irradiations carried out at higher temperatures are qualitatively similar. For example, Figs. 3**(a, b)** shows the kinetic evolution of the radiative yield for the three emission bands at 85 K. At elevated temperatures, the initial yield of the STE band shows a significantly lower intensity than that measured at 36 K, in accordance with the results reported in [32]. Above around 50–60 K, the

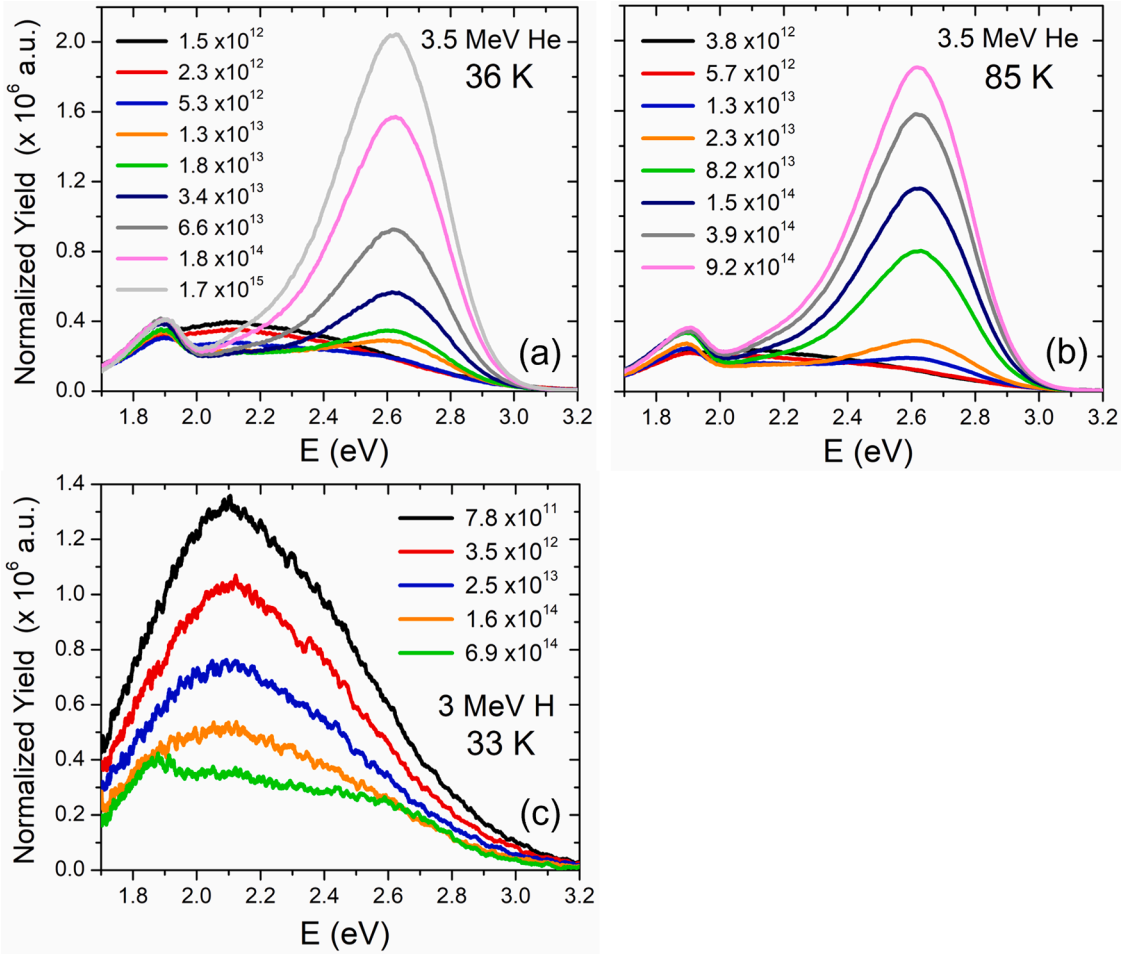

Fig. 1. Normalized luminescence spectra (in arbitrary units, a.u.) for silica irradiated at several fluences with 3.5 MeV He at 36 K (a), and 85 K (b); and with 3 MeV H at 33 K (c), for comparison. The irradiation fluences, in units of cm^{-2}, associated with each spectrum are indicated on each figure.

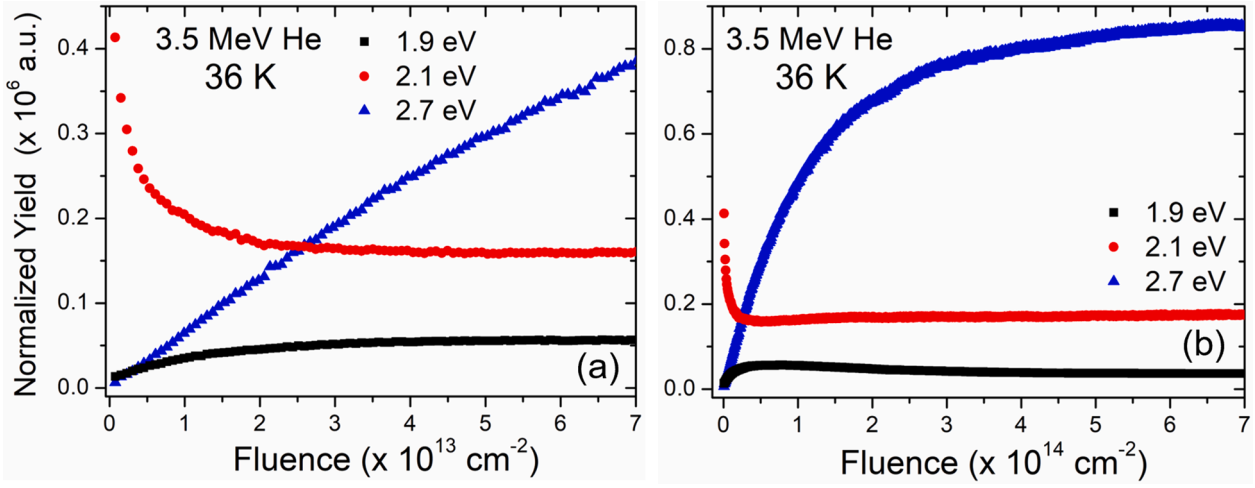

Fig. 2. Kinetics curves showing the evolution of 1.9 eV, 2.1 eV, and 2.7 eV emission band intensities as a function of 3.5 MeV He ion fluence at the lowest temperature (36 K). (a) presents, in detail, the low fluence regime, and (b) presents the behavior at higher fluences showing the saturation stage.

STEs become mobile and hop to defect sites where they non-radiatively recombine. The growth rates and saturation yields of the ODC(II) band vary little with temperature, suggesting that the kinetic behavior of this band is essentially athermal, being independent of irradiation temperature.

A) Irradiations with heavier ions, 19 MeV $Si^{6\pm}$ and $Cl^{6\pm}$. Role of electronic stopping power

IL spectra acquired under 19 MeV Si and Cl irradiation offer additional insights into the generation mechanisms and interplay among the various centers. The spectra depicted in Fig. 4**(a)** (34 K) and Fig. 4**(b)**

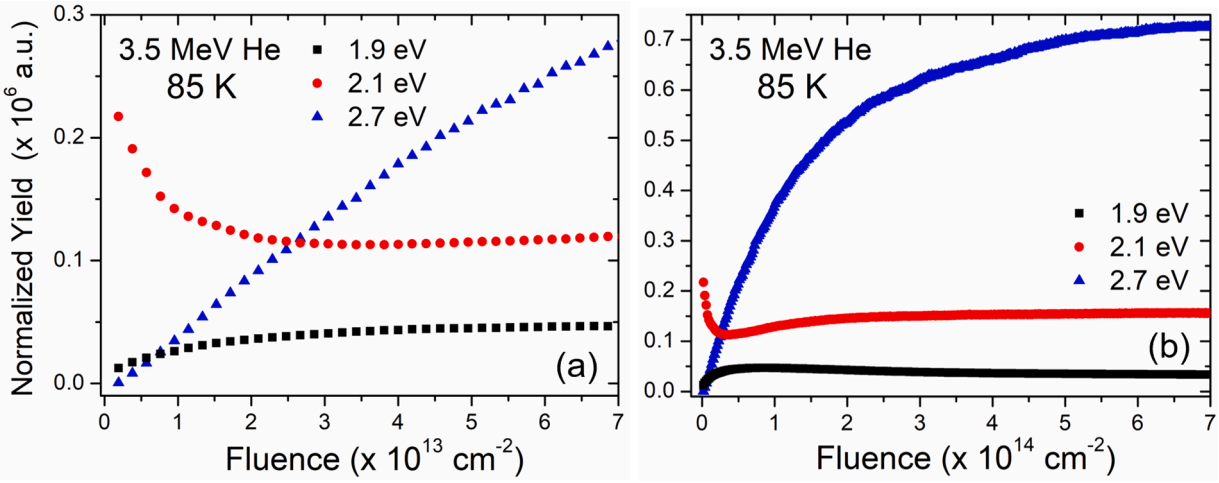

Fig. 3. Kinetics curves showing the evolution of 1.9 eV, 2.1 eV, and 2.7 eV emission band intensities as a function of 3.5 MeV He ion fluence at 85 K. (a) presents, in detail, the low fluence regime, and (b) presents the behavior at higher fluences showing the saturation stage.

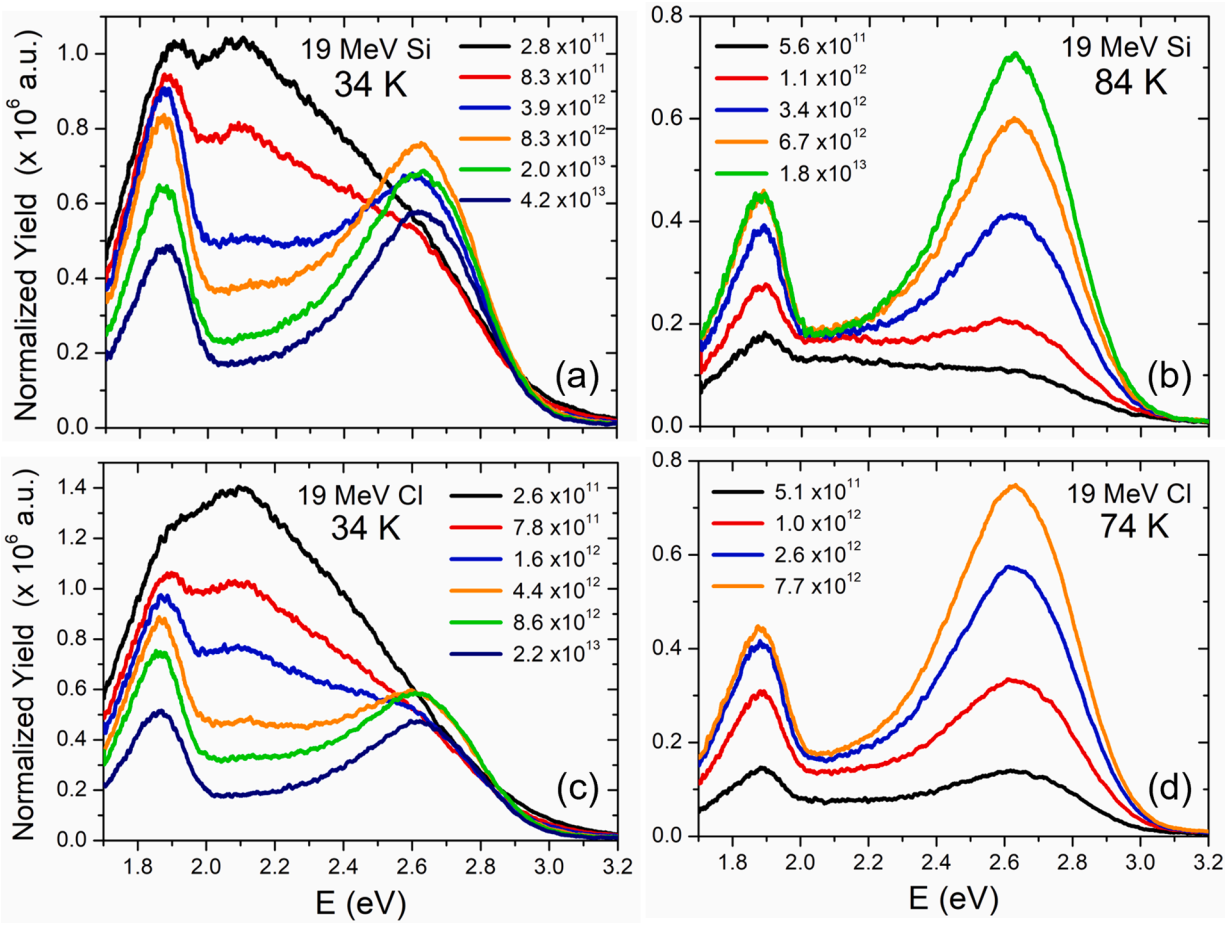

Fig. 4. Normalized luminescence spectra (in arbitrary units, a.u.) for silica irradiated at several fluences with 19 MeV Si at 34 K (a), and 84 K (b); and with 19 MeV Cl at 34 K (c), and 74 K (d), for comparison. The irradiation fluences, in units of cm^{-2}, associated with each spectrum are indicated on each figure.

(84 K) are representative of our observations. The initial spectra at 34 K and low fluences (2.8 and 8.3 $\times$ 10^{11} cm^{-2}) are again dominated by the STE (2.1 eV) band but now have a comparable contribution from the NBOHCs (1.9 eV). With increasing fluence, the STE band rapidly decreases whereas the NBOHC band changes by less than an order of magnitude. At 84 K, the STE emission yield is greatly reduced. These results indicate that the initial yields of both the STE and NBOHC bands are more intense for heavy ions than for the light ions. This suggests that the higher energy and larger stopping powers of the heavier ions play a role in the intensities of those emissions. Whether the increased intensity can be ascribed to electronic or nuclear stopping power will be discussed below.

The kinetic evolution of the radiative yields of the emission bands under 19 MeV Si irradiation are shown in Fig. 5. Spectra taken at 34 K

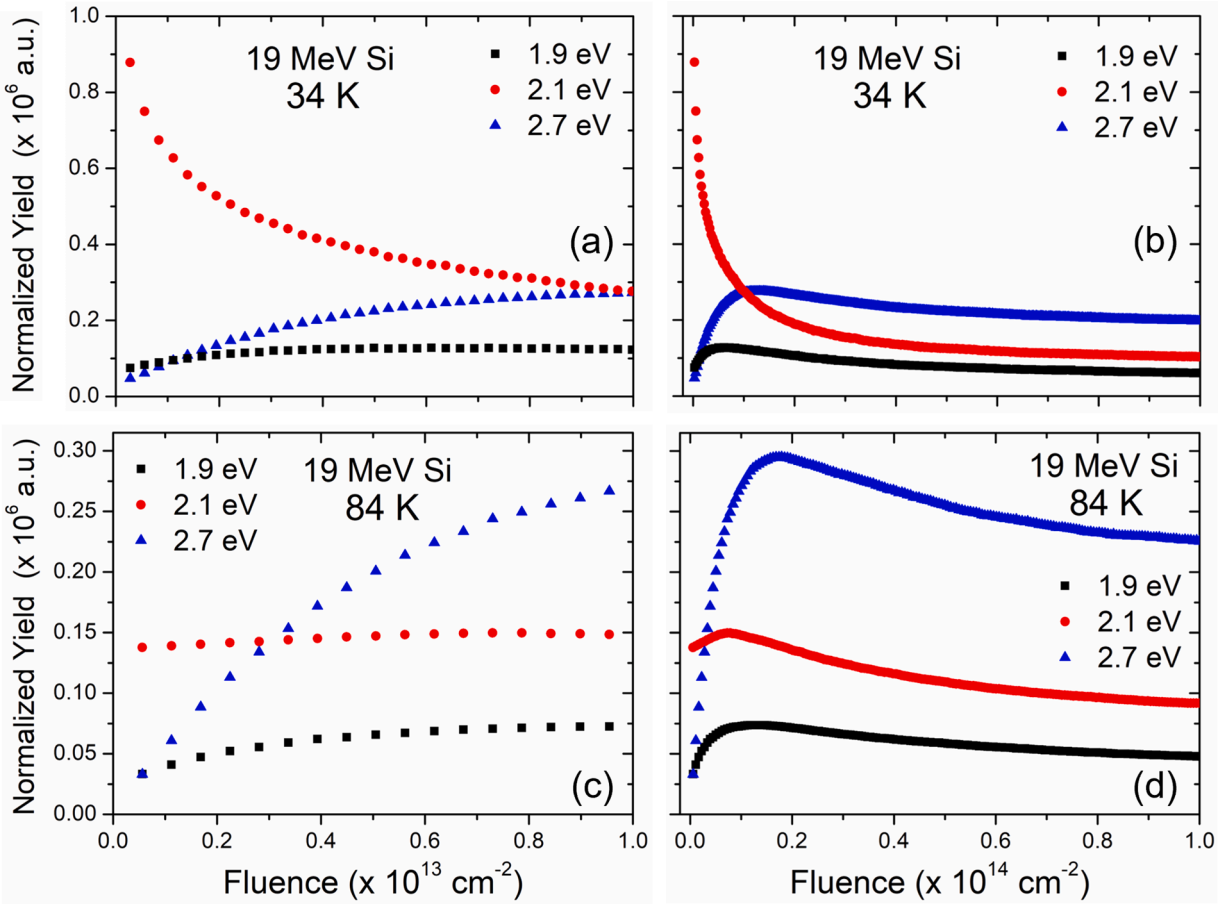

Fig. 5. Kinetics curves showing the evolution of 1.9 eV, 2.1 eV, and 2.7 eV emission band intensities as a function of 19 MeV Si ion fluence at the lowest temperature (34 K) (a, b) and at 84 K (c, d), for comparison. (a, c) present, in detail, the low fluence regime, and (b, d) present the behavior at higher fluences showing the saturation stage.

(Figs. 5**(a, b)**) and at 84 K (Figs. 5**(c, d)**) are shown for comparison. The low fluence regime is shown in Figs. 5**(a, c)**, while the high fluence regime is shown in Figs. 5**(b, d)**. At 34 K, the dominant 2.1 eV band rapidly decays with fluence, as previously discussed in [32]. The band centered at 1.9 eV (NBOHCs) shows similar behavior to that observed under light ion irradiation, i.e. there is an initial (beam-on) "jump" followed by more gradual growth that does not change by more than an order of magnitude.

Also similar to the light ion case, the band centered at 2.7 eV (ODC (II)) presents a low initial yield followed by rapid growth. The growth is linear up to around 2×10^{12} cm^{-2} (Figs. 5**(a, c)**). The intensity continues to increase sub-linearly, reaching a maximum value at around 1–2 $\times$ 10^{13} cm^{-2} (Figs. 5**(b, d)**). Notably, the onset of saturation/sub-linear growth occurs at about one order of magnitude lower fluence than for the He case. The maximum value or saturation point is also achieved at an order of magnitude lower fluence than for the case of He irradiation (Fig. 2**(b)**). At higher fluences, the OCD(II) emission yield slowly decays with fluence (Figs. 5**(b, d)**).

For irradiations carried out at the higher temperatures, the kinetics evolution with fluence for the three emission bands present similar behavior. Figs. 5**(c, d)** shows the kinetic evolution of the radiative yield for the three emissions bands at 84 K, as a representative example. As before, the STE band is considerably less intense at elevated temperature than at 34 K, in accordance with [32]. Regarding the ODC(II) emission band, the overall evolution versus irradiation fluence and maximum intensity are similar to those observed at the lowest temperature. This suggests that, as with the light ion irradiations, *the growth of the 2.7 eV band is mostly independent of irradiation temperature.* As with the light ions, the yield of the NBOHC band features a step-like intensity followed by more gradual fluence-dependent behavior. The yield in the fast initial step is higher for Si irradiation than for He.

The kinetics curves for the 1.9 eV band (NBOHC) under 19 MeV Cl irradiation at different temperatures is plotted over a range of low fluences in Fig. 6. As with the other ions, it consists of a near instantaneous

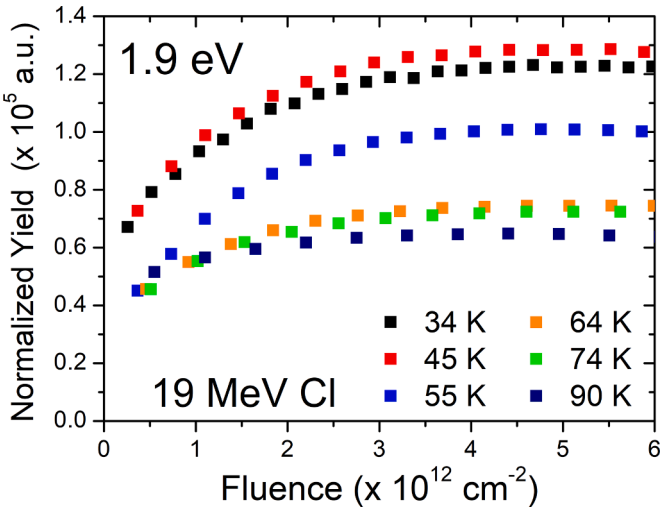

Fig. 6. Kinetics curves of the 1.9 eV (NBOHC) emission for 19 MeV Cl at low fluence for different temperatures.

(beam-on) initial contribution followed by a gradual growth stage leading to a saturation regime for fluences around 4–5 $\times$ 10^{12} cm^{-2}. It may be reasoned that the initial yield, appearing at effectively "zero" fluence and seen at all temperatures and for all ions, is inherent to the samples (i.e. it reflects the initial concentration of impurities or defects). Meanwhile, the gradual growth, which is clearly fluence dependent, can be considered radiation induced. It is possible that these inherent and induced contributions to the 1.9 eV emission band could result from the same or different processes.

To investigate the physical origin of the induced contribution, one can compare the initial yield of the 2.1 eV band to the maximum/saturation yield of the 1.9 eV band, in which the induced contribution is dominant. Fig. 7 makes this comparison over temperature for 3.5 MeV He, 19 MeV Si, and 19 MeV Cl. A correlation can be clearly observed. The decrease in yield of the 2.1 eV curve around 50–60 K has been associated with a decrease in the number of available STEs due to the activation of hopping migration of the STEs and their subsequent removal/trapping at defects [32]. Therefore, the correlation revealed in Fig. 7 suggests that the intensity of the induced component of the 1.9 eV band is related to the number of STEs.

The inherent contribution to the 1.9 eV yield will be considered next. The initial (beam-on) yield is found to be proportional to the ionizing energy, (E_{ioniz}), as illustrated in Fig. 8. The plot corresponds to the lowest irradiation temperature and includes the experimental data for all light (H, He) and heavy (Si and Cl) projectile ions. This proportionality with electronic stopping power supports the hypothesis that the mechanisms responsible for the formation of NBOH centers are purely electronic in nature (see further discussion in the next Section). When plotting the initial intensity as a function of nuclear energy loss (not shown), a similar proportionality relationship was not seen.

Regarding the ODC(II) (2.7 eV) band, the kinetics curves for 3 MeV H, 3.5 MeV He, 19 MeV Si, and 19 MeV Cl ions are shown in Fig. 9 at 33 K. The initial linear dependence with fluence up to around 10^{12} cm^{-2} can be observed, as can the strong ion mass and energy dependence. Nevertheless, the rate of growth is essentially independent of irradiation temperature (not shown). It seems, therefore, that temperature does not play a significant role in this particular emission band. Fig. 10 shows the initial growth rate (initial slope) of the 2.7 eV band vs. the number of oxygen vacancies produced per ion, for each ion at 33 K. The oxygen vacancy production rates were calculated using the SRIM simulation code (version 2012) [62,63]. The intensity of the 2.7 eV band is found to obey a simple proportionality relationship with the number of radiation-induced oxygen vacancies. A similar correlation was not seen with the ionization energy loss (not shown). These observations support the hypothesis that the physical origin of the 2.7 eV emission band is oxygen vacancies produced through a purely nuclear elastic (ballistic) origin. Furthermore, the intensity of the 2.7 eV emission band has not been normalized by the electronic carrier density. This fact and the lack of temperature dependence support a hypothesis where the ODC(II) centers are produced in an excited state and subsequently decay giving off 2.7 eV photons in the process. That is to say, the 2.7 eV emission likely does not involve the migration and trapping of carriers to the ODC (II) center (see further discussion in the next Section).

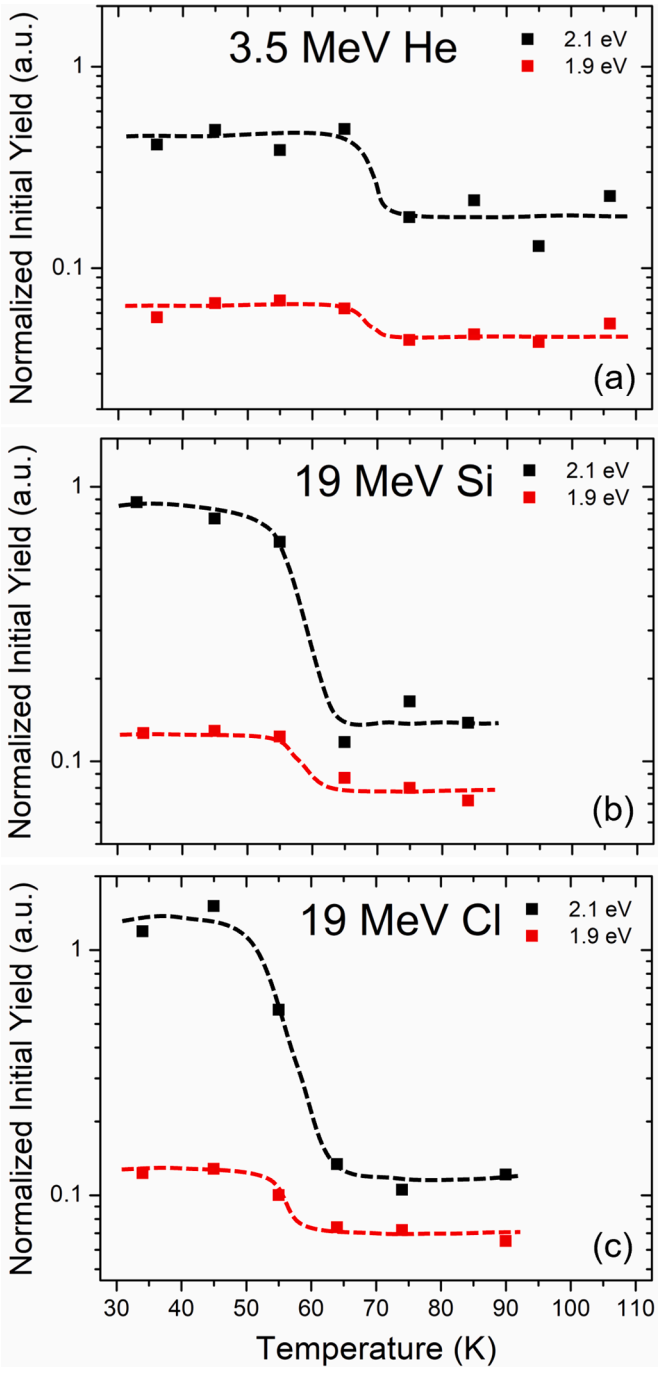

Fig. 7. The temperature dependence of the initial luminescence yield from the 2.1 eV band (STEs) and maximum/saturation yield of the 1.9 eV band (NBOH centers) for different ions (3.5 MeV He, 19 MeV Si and 19 MeV Cl). Dashed lines are included to help guide the reader's eye.

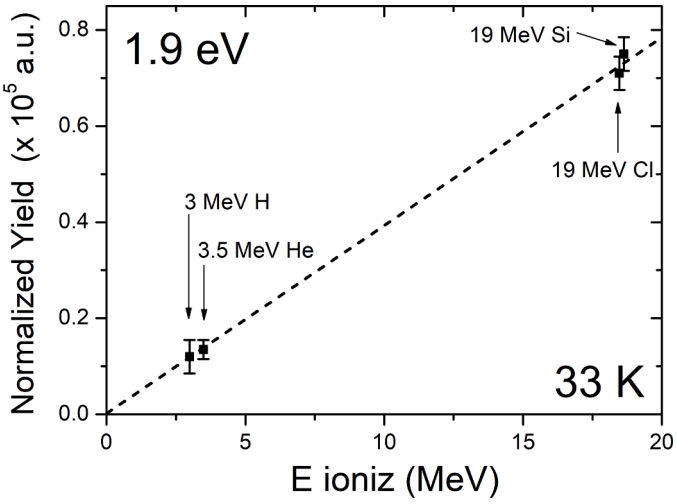

Fig. 8. Normalized initial yield intensity for the 1.9 eV emission band (NBOH centers) versus ionizing energy (E_{ioniz}) of projectile-ions at the lowest temperature, 33 K. A linear correlation can be seen between the generation of NBOH centers and the ionizing energy (E_{ioniz}).

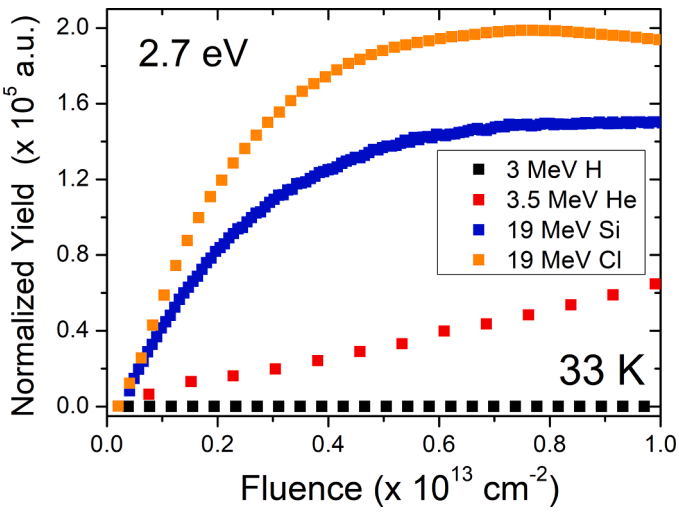

Fig. 9. Comparative kinetics, in the low fluence regime, of the evolution of the intensity of the 2.7 eV (ODC(II)) emission band with fluence at the lowest temperature (33 K), and for different ions (3 MeV H, 3.5 MeV He, 19 MeV Si and 19 MeV Cl).

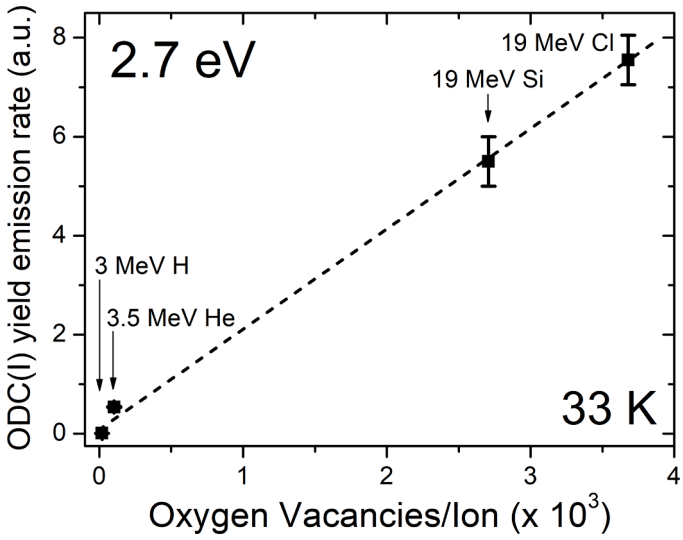

Fig. 10. 2.7 eV emission rate (slope from the initial growth of the blue luminescence intensity) as a function of the total oxygen vacancies generated per incident ion (defect generation rate calculated by SRIM code (version 2012) [62,63].) A clear linear correlation exists between the emission rate and SRIM predictions for all ions indicating a ballistic (nuclear elastic) origin of the ODC (II) centers.

3.2. Competition between electronic excitation and elastic atomic collisions during ion-beam irradiation

To summarize, the spectroscopic results presented in Section 3.1 describe three main de-excitation channels under swift ion irradiation. Electronic excitation mechanisms are associated with two of the emission bands, the 2.1 eV band (STE) and 1.9 eV band (NBOHC). In contrast, a purely collisional/ballistic mechanism has been invoked to explain the origin of the 2.7 eV band (OCD(II)).

3.2.1. Generation mechanisms for the NBOH centers (1.9 eV band)

As for the NBOHCs, the radiative emission yield centered at 1.9 eV experiences a fast initial "jump" when the beam is turned on. The fastest spectrograph shutter speed used in the measurements was 100 ms. The initial "jump" is, therefore, indicative of processes occurring on time scales of tens of ms or less. The fast jump is followed by a much more gradual growth phase until a saturation or inflection point is reached. As discussed in the previous section, the latter behavior seems to be strongly correlated with STEs, while the former is proportional to the total excitation level (number of *free* e-h pairs). In both cases however, the generation mechanism appears to be purely electronic.

While there appears to be a clear connection between the induced component of the NBOHC band and STEs, such a connection is not seen with the initial/inherent component of the NBOHC band. Fig. 11 shows the ratio between the initial component of the 1.9 eV band and the 2.1 eV band as a function of the ionization energy loss, E_{ioniz}. Where the initial/inherent contribution solely mediated by STEs, one might expect a nearly constant ratio across energy loss/ion mass. Instead, one sees a roughly linear trend. This trend mostly reflects the variation in the denominator of the ratio (i.e. STE population) with ion energy and mass in accordance with [32]. 3 MeV H irradiation, having the lowest electronic stopping power in this study, has a high STE survival fraction owing to the limited amount of Auger recombination and thermal dissociation of STEs. Therefore, STEs are the predominant carrier formed and, consequently, the ratio has a large denominator for swift protons. For the heavy ions, previous works [32,68,69] discuss how the internal core of the ion tracks reach much higher temperatures, excitation densities, and are possibly more defective than the outside ring (shell). This results in a dramatic reduction of the surviving fraction of STEs inside the track due to competition from non-radiative recombination. The resulting denominator in the ratio is small. At the same time, the higher electronic stopping power of the heavy energetic ions allows for a high rate of initial/inherent NBOHC stimulation per ion (Fig. 8). Considering these facts together, the yield of the initial/inherent NBOH centers is likely related to *free* and not to *self-trapped* carriers, as suggested in a previous work where ion-beam irradiations were conducted at room temperature (RT) [30,31].

One may consider two mechanisms of NBOHC generation: 1) scission of strained ($\equiv Si-O-Si\equiv$) bonds [42,43], and 2) scission of silanol groups ($\equiv Si-O-H \rightarrow \equiv Si-O^{\bullet} + H$) [70,71] after free electron trapping. The behavior of the initial/inherent contribution to the NBOHC band appears to be more consistent with the second mechanism. The intensity obtained is proportional to the excitation level (hence free electron concentration). Assuming trapping of free electrons by a field of OH impurities follows unimolecular kinetics and that trapping is not

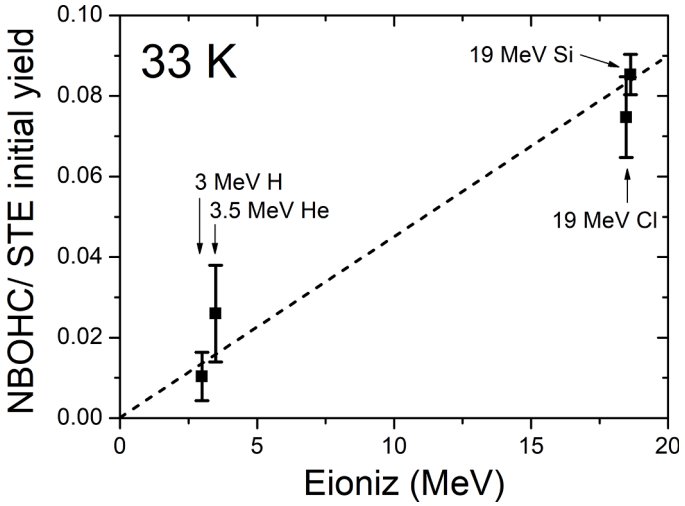

Fig. 11. Ratio of the initial/intrinsic component of the NBOHC (1.9 eV) band intensity to the 2.1 eV emission band intensity (STE centers) plotted as a function of ionizing energy (E_{ioniz}). The positive linear correlation with ionizing energy reflects both the higher per ion rate of NBOHC production seen at higher ionizing energies as well as the lower STE survival probability associated with heavier ions.

diffusion limited, one would expect a proportional relationship between NBOHC yield and free electron concentration. This is also supported by previous ion-beam irradiations at RT on samples having different silanol contents [30]. Therefore, the initial abrupt jump observed in the yield for the red luminescence band could be interpreted as the radiative decay of the *excited state/antibonding state* of the silanol group.

The other mechanism mentioned involves the breaking of strained ($\equiv Si-O-Si\equiv$) bonds contributing to the formation of NBOH centers. It can be described by the equation $\equiv Si-O-Si\equiv \rightarrow \equiv Si-O^{\bullet} + \equiv Si^{\bullet}$, culminating in the creation of a coupled E′ ($\equiv Si^{\bullet}$) and NBOH center ($\equiv Si-O^{\bullet}$) pair (also see Eq. (3) in [30]). This mechanism, which requires no impurities to occur, could help explain the induced (fluence dependent) contribution to the 1.9 eV emission band. It is reasonable to expect ion beam induced damage to result in the formation of strained bonds. However, the relative magnitude of the extrinsic contribution is the same for light and heavy ions (compare for example the 1.9 eV kinetics curves in Figs. 2 and 6). It is therefore unlikely that atomic restructuring can wholly account for bond strain. On the other hand, STEs, which are apparently correlated with the induced portion of the NBOHC band, may produce strained bonds and therefore act as precursors to the above decay equation [72]. The decrease in intensity of the 2.1 eV band with temperature has been attributed to the thermal activation of STE hopping migration to non-luminescent defect centers where they recombine non-radiatively [32]. It stands to reason then that competitive recombination at non-luminescent centers also governs, to some extent, the generation rate of irradiation induced NBOHCs.

Two NBOHC formation mechanisms are proposed here to explain the observed kinetic behavior. It would be useful to also examine the formation of E′ centers to assess the contribution of the strained bond channel, if any. Correlation of the E' concentration with ion fluence, OH impurity concentration, and STE emission intensity would help verify that STEs are indeed the main precursor to the induced component, while silanol groups determine the initial luminescence yield.

3.2.2. *Generation mechanisms for the ODC(II) centers (2.7 eV band): correlation with oxygen vacancies production simulated by SRIM code*

The growth rate (slope) of the emission band centered at 2.7 eV is essentially proportional to the oxygen vacancy production rate as calculated by SRIM (version 2012) [62,63]. The strong linear correlation and lack of temperature dependence makes the association with a ballistic process fairly unambiguous. At variance with previous analysis done on the perovskite $SrTiO_3$, where an oxygen vacancy band at 2.0 eV showed similar linear dependence on fluence [51], no correction factor was applied to silica to account for the carrier density ($\rho_{e\text{-}h}$) or electronic stopping power (S_e). In $SrTiO_3$, it was assumed that the oxygen vacancies were created in their ground state and subsequently trapped electrons. In silica, where the carrier density normalization was not performed, the situation seems different. ODCs are created in an excited state and therefore do not need to first capture electrons in order to emit 2.7 eV photons. The nuclear elastic collision itself appears to provide the electronic excitation energy within the defect. In the linear correlation seen in Fig. 10 and the absence of any clear temperature-dependence strongly suggest that, at least for the temperature and irradiation conditions considered in this study, there is no additional electron re-trapping required for light emission.

At high fluences (above 5–6 $\times$ 10^{14} cm^{-2} for light (H, He) ions and above 2 $\times$ 10^{13} cm^{-2} for heavy (Si, Cl) ions), as shown in Figs. 2**(b),** 3**(b) and** 5**(b, d)**), there is clear evidence of saturation of the OCD(II) emission band. The onset of saturation appears to depend on ion mass and irradiation temperature. The largest variation is observed between light (H, He) and heavy ions (Si, Cl). The kinetics curves for light ions experience a monotonic growth and saturate; whereas for heavy ions, the yield initially grows to reach a maximum value and then decreases. Similar behavior was reported in irradiation experiments conducted with heavy ions at RT. The radiative emission process is sensitive to structural disorder produced under irradiation [30,31]. Those previous works proposed that the growth and decay behavior was related to structural effects associated with the electronic stopping power (S_e) and not due to collisional (elastic recoil) effects. Ion induced compaction effects (structural disorder) of the silica network have also been investigated in detail using infra-red (IR) absorption spectroscopy [73]. Awazu et al. [73] revealed that the frequency of the first-order ω_4 vibrational mode of Si-O-Si bonds, associated with the silica network compaction (asymmetric stretching of the bond) changed under SHI irradiation but not for light ion irradiation. Moreover, the onset of observable structural changes began at lower fluences for higher stopping powers [30,31,73]. This behavior parallels the one observed in IL spectra below 100 K, which show that the point where the 2.7 eV band begins to decrease in intensity appears at progressively lower fluences as stopping power increases. Thus, the observed saturation and decrease in intensity of the OCD(II) band might be related to enhanced non-radiative decay associated with network compaction with the caveat that results from IR measurements performed on silica irradiated at RT are not necessarily transferable to experiments conducted at LT. Future IR measurements of silica irradiated at cryogenic temperature may help corroborate this hypothesis.

In any case, it is interesting to consider correlating the luminescence emissions to the structural modification of silica (ring configurations) during irradiation. Undoubtfully, future work should examine the competition between radiative and non-radiative recombination in the overlapping track regime. The compaction effect illustrates the complexities of ion-beam irradiation in comparison with purely ionizing irradiation, such as provided by synchrotron or laser sources. Overall, cryo-ionoluminescence offers further insight into the electronic (excitonic) and nuclear origins of optically active defects in silica.

4. Summary and conclusions

The results presented and discussed in this work establish the production mechanisms for each of the three, well-known, emission bands centered at 1.9 eV, 2.1 eV and 2.7 eV in silica under energetic ion irradiation and at temperatures in the range 30 to 100 K. The kinetic evolution of highly overlapping NBOHC band (1.9 eV), STE band (2.1 eV), and OCD(II) band (2.7 eV) is made possible by separating the emissions, not in energy, but using fluence and temperature. Ionoluminescence (IL) is a powerful technique that presents a number of advantages for the comprehensive analysis of luminescence centers, providing real-time *in-situ* information. It combines electronic excitation processes within a broad energy spectrum with structural modification (damage) by collisional processes allowing one to identify centers as being electronic in origin or structural in origin. Furthermore, intrinsic vs. extrinsic defects and centers can be differentiated in a straightforward way through the study of kinetics curves. Variation of the intensities and kinetics of various radiative emission bands with temperature, ion mass, and energy aids in the determination of the generation mechanisms, structure, and kinetic evolution of their corresponding luminescence centers. Therefore, cryo-ionoluminescence has provided a glimpse into the physical origins of defect production in silica under ion irradiation. The generation of NBOH and OCD(II) centers follow different processes. NBOH centers are created through electronic excitation and may be produced both through bond-scission of silanol groups (from OH impurities) or through the decay of strained Si-O bonds associated with STEs. The role of temperature on the kinetic evolution of the red (1.9 eV) emission band reveals that a relationship likely exists between the NBOH centers and STE centers. Decomposition of STEs into E' centers and NBOHCs is currently the most plausible explanation for the induced growth of the NBOHC band. STEs themselves carry energy from the initial ion-solid interaction to the atomic structure and thus play an important role in determining the microscopic and macroscopic effects of ion-irradiation in silica. In contrast to the electronically generated STEs and NBOCs, the ODC(II) centers are produced through athermal ion-atom elastic collision processes. This was seen through the

strong linear correlation between blue emission rate of the 2.7 eV band with SRIM radiation damage calculations. The linear correlation is seen without normalization by carrier density, suggesting that the oxygen vacancy centers are produced in an excited state and de-excite spontaneously rather than by first trapping an electron. At high irradiation fluences, the initial linear growth stage of the 2.7 eV emission band transitions to a saturation regime before decaying (heavy ions). In accordance with results by Awazu et al. [73] at RT, the decay stage may be attributed to silica network compaction. Future work should examine the competition between radiative and non-radiative recombination in the overlapping track regime. In summary, the results and analysis in this paper provide a complete picture of the effects of ion-beam irradiation on silica, and particularly on the interplay between the various induced luminescence centers and their generation mechanisms. The present study pertains to the radiation response of bulk glass. The results may differ in non-bulk systems such as optical fibers or nanostructured glass [50]. Furthermore, this work highlights how ionoluminescence can be used as a real-time spectroscopic tool to untangle complex irradiation-induced processes, allowing one to identify the main routes for the energy transfer from the incident particle through to the electronic and atomic structure.

Data availability statement

The data that support the findings of this study are available from the corresponding author upon reasonable request.

Declaration of Competing Interest

The authors declare that they have no known competing financial interests or personal relationships that could have appeared to influence the work reported in this paper.

Acknowledgments

M.L. Crespillo acknowledges financial support from the University of Tennessee Governor's Chair program and the research project "Captación de Talento UAM" Ref: #541D300 supervised by the Vice-Chancellor of Research of Universidad Autónoma de Madrid (UAM). The contribution of W.J. Weber was supported by the National Science Foundation under Grant No. DMR-2104228.

Supplementary materials

Supplementary material associated with this article can be found, in the online version, at doi:10.1016/j.actamat.2023.119097.

References

[1] L. Tong, R. Gattass, J. Ashcom, S. He, J. Lou, M. Shen, I. Maxwell, E. Mazur, Subwavelength-diameter silica wires for low-loss optical wave guiding, Nature 426 (2003) 816–819.
[2] M. Lancry, B. Poumellec, UV laser processing and multiphoton absorption processes in optical telecommunication fiber materials, Phys. Rep. 523 (2013) 207–229.
[3] J. Manzano-Santamaría, J. Olivares, F. Agulló-López, M.L. Crespillo, A. Moroño, E. Hodgson, Optical waveguides obtained by swift-ion irradiation on silica (a-SiO_2) Nucl, Instrum. Methods B 268 (2010) 3147–3150.
[4] W.J. Weber, R.C. Ewing, C.A. Angell, et al., Radiation effects in glasses used for immobilization of high-level waste and plutonium disposition, J. Mater. Res. 12 (1997) 1948–1978.
[5] A. Ibarra, E.R. Hodgson, The ITER project: the role of insulators, Nucl. Instrum. Methods Phys. Res. B 218 (2004) 29–35.
[6] J.F. Latkowski, A. Kubota, M.J. Caturla, S.N. Dixit, J.A. Speth, S.A. Payne, Fused silica final optics for inertial fusion energy: radiation studies and system-level analysis, Fusion Sci. Technol. 43 (2003) 540–558.
[7] L. Skuja, M. Hirano, H. Hosono, K. Kajihara, Defects in oxide glasses, Phys. Stat. Sol. C 2 (2005) 15–24.
[8] F. Messina, L. Vaccaro, M. Cannas, Generation and excitation of point defects in silica by synchrotron radiation above the absorption edge, Phys. Rev. B 81 (2010), 035212.
[9] R. Salh, Defect related luminescence in silicon dioxide network: a review, in: S Basu (Ed.), Crystalline Silicon - Properties and Uses, InTech, Rijeka, 2011, pp. 135–172, pp. 135-172.
[10] F. Agulló-López, C.R. Catlow, P.D. Townsend, Point Defects in Materials, Academic Press, London, 1984. Academic Press, London.
[11] N. Itoh, M. Stoneham, Materials Modification By Electronic Excitation, Cambridge University Press, Cambridge, U.K., 2000.
[12] C.D. Marshall, J.A. Speth, S.A. Payne, Induced optical absorption in gamma, neutron and ultraviolet irradiated fused quartz and silica, J. Non-Cryst. Solids 212 (1997) 59–73.
[13] A. Paleari, F. Meinardi, S. Brovelli, R. Lorenzi, Competition between green self-trapped-exciton and red non-bridging-oxygen emissions in SiO2 under interband excitation, Commun. Phys. 1 (2018) 67.
[14] A. Moroño, E.R. Hodgson, Radiation induced optical absorption and radioluminescence in electron irradiated SiO_2, J. Nucl. Mater. 258-263 (1998) 1889–1892.
[15] K. Tanimura, T. Tanaka, N. Itoh, Creation of quasistable lattice defects by electronic excitation in SiO_2, Phys. Rev. Lett. 51 (1983) 423.
[16] M. Leon, P. Martín, A. Ibarra, E.R. Hodgson, Gamma irradiation induced defects in different types of fused silica, J. Nucl. Mater. 386–388 (2009) 1034–1037.
[17] A.K. Islamov, U.S. Salikhbaev, E.M. Ibragimova, et al., Efficiency of generation of optical centers in KS-4V and KU-1 quartz glasses at neutron and gamma irradiation, J. Nucl. Mater. 443 (2013) 393–397.
[18] M. León, P. Martín, R. Vila, J. Molla, A. Ibarra, Vacuum ultraviolet excitation of the 2.7eV emission band in neutron irradiated silica, J. Non-Cryst. Sol. 355 (2009) 1034–1037.
[19] M. Leon, L. Giacomazzi, S. Girard, N. Richard, P. Martín, L. Martín-Samos, A. Ibarra, A. Boukenter, Y. Ouerdane, Neutron irradiation effects on the structural properties of KU1, KS-4V and I301 silica glasses, IEEE Trans. Nucl. Sci. 61 (2014) 1522.
[20] P.D. Townsend, P.J. Chandler, L. Zhang, Optical Effects of Ion Implantation (Cambridge Studies in Modern Optics), Cambridge University Press, UK, Cambridge, (UK), 1994 (chapters 4 & 5).
[21] S. Nagata, S. Yamamoto, K. Toh, B. Tsuchiya, N. Ohtsu, T. Shikama, H. Naramoto, Luminescence in SiO_2 induced by MeV energy proton irradiation, J. Nucl. Mater. 329–333 (2004) 1507–1510.
[22] S. Nagata, S. Yamamoto, A. Inouye, B. Tsuchiya, K. Toh, T. Shikama, Luminescence characteristics and defect formation in silica glasses under H and He ion irradiation, J. Nucl. Mater. 367–370 (2007) 1009–1013.
[23] S. Nagata, H. Katsui, B. Tsuchiya, A. Inouye, S. Yamamoto, K. Toh, T. Shikma, Damage process and luminescent characteristics in silica glasses under ion irradiation, J. Nucl. Mater. 386-388 (2009) 1045–1048.
[24] F. Agulló-López, A. Climent-Font, A. Muñoz-Martin, J. Olivares, A. Zucchiatti, Ion beam modification of dielectric materials in the electronic excitation regime: cumulative and exciton models, Prog. Mater. Sci. 76 (2016) 1–58.
[25] M.L. Crespillo, J.T. Graham, Y. Zhang, W.J. Weber, In-situ luminescence monitoring of ion-induced damage evolution in SiO_2 and Al_2O_3, J. Lumin. 172 (2016) 208–218.
[26] J. Manzano-Santamaría, J. Olivares, A. Rivera, O. Peña-Rodríguez, F. Agulló-López, Kinetics of color center formation in silica irradiated with swift heavy ions: thresholding and formation efficiency, Appl. Phys. Lett. 101 (2012), 154103.
[27] D. Jimenez-Rey, O. Peña-Rodríguez, J. Manzano-Santamaría, J. Olivares, A. Muñoz-Martin, A. Rivera, F. Agulló-López, Ionoluminescence induced by swift heavy ions in silica and quartz: a comparative analysis, Nucl. Instrum. Methods B 286 (2012) 282–286.
[28] O. Peña-Rodriguez, J. Manzano-Santamaría, J. Olivares, A. Rivera, F. Agullo-Lopez, Refractive index changes in amorphous SiO2 (silica) by swift ion irradiation, Nucl. Instrum. Methods Phys. Res. B 277 (2012) 126–130.
[29] R. Saavedra, P. Martin, D. Jimenez-Rey, R. Vila, Structural changes induced in silica by ion irradiation observed by IR reflectance spectroscopy, Fusion Eng. Des. 98–99 (2015) 2034–2037.
[30] D. Bachiller-Perea, D. Jimenez-Rey, A. Muñoz-Martin, F. Agulló-López, Ion beam induced luminescence in amorphous silica: role of the silanol group content and the ion stopping power, J. Non-Cryst. Solids 428 (2015) 36–41.
[31] D. Bachiller-Perea, D. Jiménez-Rey, A. Muñoz-Martín, F Agulló-López, Exciton mechanisms and modeling of the ionoluminescence in silica, J. Phys. D 49 (2016), 085501.
[32] J.T. Graham, M.L. Crespillo, F. Agulló-López, W.J. Weber, Light emission of self-trapped excitons from ion tracks in silica glass: interplay between Auger recombination, exciton formation, thermal dissociation, and hopping, Acta Mater. 229 (2022), 117829.
[33] M.L. Crespillo, J.T. Graham, F. Agulló-López, Y. Zhang, W.J. Weber, Role of oxygen vacancies on light emission mechanisms in $SrTiO_3$ induced by high-energy particles, J. Phys. D 50 (2017), 155303.
[34] P.D. Townsend, M. Khanlary, D.E Hole, Information obtainable from ion beam luminescence, Surf. Coat. Technol. 201 (2007) 8160–8164.
[35] P.D. Townsend, M.L. Crespillo, An ideal system for analysis and interpretation of ion beam induced luminescence, Phys. Procedia 66 (2015) 345–351.
[36] K. Kajihara, M. Hirano, L. Skuja, H. Hosono, Intrinsic defect formation in amorphous SiO_2 by electronic excitation: bond dissociation versus Frenkel mechanisms, Phys. Rev. B 78 (2008), 094201.
[37] L. Skuja, Optically active oxygen-deficiency-related centers in amorphous silicon dioxide, J. Non-Cryst. Solids 239 (1998) 16.
[38] S. Ismail-Beigi, S.G. Louie, Self-trapped excitons in silicon dioxide: mechanism and properties, Phys. Rev. Lett. 95 (2005), 156401.

[39] K.S. Song, R.T. Williams, Self-Trapped Excitons (Springer Series in Solid-State Sciences), Springer-Verlag Berlin, Heidelberg, 1993.
[40] R.M. Van Ginhoven, H. Jónsson, L.R. Corrales, Characterization of exciton self-trapping in amorphous silica, J. Non-Cryst. Sol. 352 (2006) 2589–2595.
[41] M.A. Stevens-Kalceff, Cathodoluminescence microcharacterization of point defects in alpha-quartz, Mineral. Mag. 73 (2009) 585–605.
[42] T.E. Tsai, D.L. Griscom, Experimental evidence for excitonic mechanism of defect generation in high-purity silica, Phys. Rev. Lett. 67 (1991) 2517–2520.
[43] H. Hosono, Y. Ikuta, T. Kinoshita, K. Kajihara, M. Hirano, Physical disorder and optical properties in the vacuum ultraviolet region of amorphous SiO_2, Phys. Rev. Lett. 87 (2001), 175501.
[44] R.A.B. Devine, J. Arndt, Defect pair creation through ultraviolet radiation in dense, amorphous SiO_2, Phys. Rev. B 42 (1990) 2617 (R).
[45] R.A.B. Devine, Physics and Technology of Amorphous SiO_2, Springer, Boston, USA, 1988.
[46] A.N. Trukhin, Luminescence of localized states in silicon dioxide glass. A short review, J. Non-Cryst. Solids 357 (2011) 1931–1940.
[47] L. Skuja, Optical properties of defects in silica, in: G. Pacchioni, L. Skuja, D. L. Griscom (Eds.), Defects in and Related Dielectrics: Science and Technology (NATO Science Series II), Kluwer, Dordrecht, The Netherlands, 2000, pp. 73–116.
[48] H. Nishikawa, E. Watanabe, D. Ito, Y. Ohki, Decay kinetics of the 4.4-eV photoluminescence associated with the two states of oxygen-deficient-type defect in amorphous SiO_2, Phys. Rev. Lett. 72 (1994) 2101.
[49] D. Bachiller-Perea, PhD Thesis. Ion-Irradiation-Induced Damage in Nuclear Materials: Case Study of a-SiO_2 and MgO. Springer Theses, Recognizing Outstanding Ph. D. Research, ISSN 2190-5053, Springer International Publishing, 2018.
[50] S. Girard, et al., Overview of radiation induced point defects in silica-based optical fibers, Rev. Phys. 4 (2019), 100032.
[51] M.L. Crespillo, J.T. Graham, F. Agulló-López, Y. Zhang, W.J. Weber, Isolated oxygen vacancies in strontium titanate shine red: optical identification of Ti^{3+} polarons, Appl. Mater. Today 12C (2018) 131–137.
[52] M.L. Crespillo, J.T. Graham, F. Agulló-López, Y. Zhang, W.J. Weber, Correlation between Cr^{3+} luminescence and vacancy disorder under MeV ion irradiation, J. Phys. Chem. C 121 (2017) 19758–19766.
[53] M.L. Crespillo, J.T. Graham, F. Agulló-López, Y. Zhang, W.J. Weber, The blue emission at 2.8eV in strontium titanate: evidence for a radiative transition of self-trapped excitons from unbound states, Mater. Res. Lett. 7 (2019) 298–303.
[54] M.L. Crespillo, J.T. Graham, F. Agulló-López, Y. Zhang, W.J. Weber, Recent advances on carrier and exciton self-trapping in strontium titanate: understanding the luminescence emissions, Crystals 9 (2019) 95.
[55] M.L. Crespillo, J.T. Graham, F. Agulló-López, Y. Zhang, W.J. Weber, Non-radiative luminescence decay with self-trapped hole migration in strontium titanate: interplay between optical and transport properties, Appl. Mater. Today 23 (2021), 101041.
[56] M.L. Crespillo, J.T. Graham, F. Agulló-López, Y. Zhang, W.J. Weber, Real-time identification of oxygen vacancy centers in $LiNbO_3$ and $SrTiO_3$ during irradiation with high energy particles, Crystals 11 (2021) 315.
[57] O. Peña-Rodríguez, M.L. Crespillo, P. Díaz-Nuñez, J.M. Perlado, A. Rivera, J. Olivares, In situ monitoring the optical properties of dielectric materials during ion irradiation, Opt. Mater. Express 6 (2016) 734–742.
[58] O. Pena-Rodrıguez, D. Jimenez-Rey, J. Manzano-Santamarıa, J. Olivares, A. Munoz, A. Rivera, F. Agullo-Lopez, Ionoluminescence as sensor of structural disorder in crystalline SiO_2: determination of amorphization threshold by swift heavy ions, Appl. Phys. Express 5 (2012), 011101.
[59] www.crystran.co.uk/.
[60] Y. Zhang, M.L. Crespillo, H. Xue, K. Jin, C.H. Chen, C.L. Fontana, J.T. Graham, W. J. Weber, New ion beam materials laboratory for effective investigation of materials modification and irradiation effects, Nucl. Instrum. Methods B 338 (2014) 19–30.
[61] M.L. Crespillo, J.T. Graham, Y. Zhang, W.J. Weber, Temperature measurements during high flux ion beam irradiations, Rev. Sci. Instrum. 87 (2016), 024902.
[62] J.F. Ziegler, M.D. Ziegler, J.P. Biersack, SRIM—the stopping and range of ions in matter, Nucl. Instrum. Methods B 268 (2010), 1818-1123.
[63] J.F. Ziegler. Software code. SRIM (v2012)-The Stopping and Range of Ions in Matter, Software code. SRIM (v2012)-The Stopping and Range of Ions in Matter (2012).
[64] R.C. Hughes, Charge-carrier transport phenomena in amorphous SiO_2: direct measurement of the drift mobility and lifetime, Phys. Rev. Lett. 30 (1973) 1333.
[65] F.S. Goulding, Y. Stone, Semiconductor radiation detectors, Science 170 (1970) 280–289.
[66] M. Wojdyr, Fityk: a general-purpose peak fitting program, J. Appl. Crystallogr. 43 (2010) 1126.
[67] J. Wolberg, Data Analysis Using the Method of Least Squares: Extracting the Most Information from Experiments, Springer, 2006.
[68] K. Michaelian, A. Menchaca-Rocha, Model of ion-induced luminescence based on energy deposition by secondary electrons, Phys. Rev. B 49 (1994) 15550.
[69] L. Muga, G. Griffith, Specific luminescence studies in plastic scintillators, Phys. Rev. B 9 (1974) 3639.
[70] K. Kajihara, L. Skuja, M. Hirano, H. Hosono, Formation and decay of nonbridging oxygen hole centers in SiO2 glasses induced by F_2 laser irradiation: in situ observation using a pump and probe technique, Appl. Phys. Lett. 79 (2001) 1757–1759.
[71] K. Kajihara, Y. Ikuta, M. Hirano, T. Ichimura, H. Hosono, Interaction of F_2 excimer laser pulses with hydroxy groups in SiO_2 glass: hydrogen bond formation and bleaching of vacuum ultraviolet absorption edge, J. Chem. Phys. 115 (2001) 9473–9476.
[72] K. Mishchik, Ultrafast Laser-Induced Modification of Optical Glasses: a Spectroscopy Insight Into the Microscopic Mechanisms, Université Jean Monnet - Saint-Etienne, 2014 vol. Ph.D.
[73] K. Awazu, S. Ishii, K. Shima, S. Roorda, J.L. Brebner, Structure of latent tracks created by swift heavy-ion bombardment of amorphous SiO_2, Phys. Rev. B 62 (2000) 3689–3698.